

Phase Diagrams and Energy Barriers of Exchange-biased Bilayers  
with Additional Anisotropies in the Ferromagnet

T. Mewes – University of Kaiserslautern

H. Nembach – University of Kaiserslautern

J. Fassbender – University of Kaiserslautern

B. Hillebrands – University of Kaiserslautern

Joo-Von Kim – University of Western Australia

R. L. Stamps – University of Western Australia

Deposited 08/28/2018

Citation of published version:

Mewes, T., Nembach, H., Fassbender, J., Hillebrands, B., Kim, J., Stamps, R. (2003): Phase Diagrams and Energy Barriers of Exchange-biased Bilayers with Additional Anisotropies in the Ferromagnet, *Physical Review B*, vol. 67. <https://doi.org/10.1103/PhysRevB.67.104422>

# Phase diagrams and energy barriers of exchange-biased bilayers with additional anisotropies in the ferromagnet

T. Mewes, H. Nembach, J. Fassbender, and B. Hillebrands

*Fachbereich Physik and Forschungs- und Entwicklungsschwerpunkt Materialwissenschaften, Universität Kaiserslautern, D-67663 Kaiserslautern, Germany*

Joo-Von Kim and R. L. Stamps

*School of Physics, University of Western Australia, 35 Stirling Highway, Crawley, WA 6009, Australia*

(Received 18 June 2002; revised manuscript received 5 November 2002; published 21 March 2003)

A general discussion of magnetization in exchange-biased bilayers with higher-order anisotropy contributions in an applied magnetic field is given. Allowed magnetic configurations for a ferromagnet in an applied magnetic field are shown in magnetic phase diagrams that illustrate competing effects of unidirectional, uniaxial, and fourfold anisotropies. The role and asymmetry of energy barriers during magnetization reversal are discussed in detail. A direct comparison with recent experimental results in epitaxial NiFe/FeMn bilayers is provided, and the influence of thermal activation on the magnetization reversal process is discussed.

DOI: 10.1103/PhysRevB.67.104422

PACS number(s): 75.30.Gw, 75.70.-i, 75.60.Jk, 75.40.Mg

## I. INTRODUCTION

The exchange-bias effect was discovered more than forty years ago by Meiklejohn and Bean.<sup>1,2</sup> The complexity of competing interactions involved in the formation of exchange bias is responsible for a variety of interesting phenomena that have not been successfully quantified in over forty years of research. Details concerning the microscopic origin remain a subject of active research and discussion, and there are several recent reviews of the current status.<sup>3-5</sup> Meiklejohn and Bean proposed the first explanation of exchange bias within a modified Stoner-Wohlfarth model<sup>6</sup> with bias ultimately created by unidirectional anisotropy associated with the ferromagnet/antiferromagnet interface.

Because of experimental results that have appeared since, it has been widely accepted that a simple description based on unidirectional anisotropy only cannot account for the wide variety of observed phenomena associated with the exchange bias. The increased coercivity and associated angular dependence that is observed in exchange-bias systems suggest that higher-order effective anisotropies are present, for example. We show that the inclusion of uniaxial<sup>7-10</sup> and fourfold<sup>10-13</sup> anisotropy contributions in addition to the unidirectional anisotropy are sufficient to describe the complex angular dependence observed in biased NiFe/FeMn bilayers.

A type of phase diagram was shown to be a useful tool for describing applied field controlled magnetic ordering in uniaxial ferromagnets.<sup>14,15</sup> In this paper we extend the idea to magnetic heterostructures and present a detailed analysis of the magnetic ordering in exchange-biased bilayers.

## II. THE MODEL

### A. Introduction

In order to explain the meaning of the diagrams we will use to discuss ordering according to magnetic phases, we first consider the ideal case of a ferromagnet with only a unidirectional anisotropy. If the external field  $H$  is applied

along the easy direction of the unidirectional anisotropy, the hysteresis curve is shifted along the field axis and exhibits a sudden jump at the exchange-bias field as shown in Fig. 1(a). The dependence of the magnetization reversal on the strength of the unidirectional anisotropy is visualized in the phase diagram given in Fig. 1(b). As the free enthalpy of the system always has exactly one minimum the phase diagram in this configuration consists only of two regions. These regions correspond to parallel and antiparallel alignment of the magnetization with respect to the easy direction of the unidirectional anisotropy  $e_1$ . In this diagram, the white filling indicates parallel alignment, and black filling indicates antiparallel alignment.

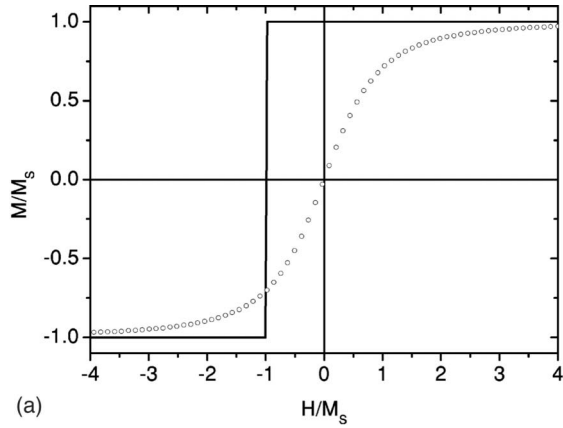
Application of the external field perpendicular to the easy direction of the unidirectional anisotropy results in an unshifted loop without coercivity as shown in Fig. 1(a). The magnetization rotates continuously into the direction of the applied field, and the corresponding phase diagram does not exhibit any sharp boundaries but instead shows a continuous variation from white to black across the zero applied field line as can be seen in Fig. 1(c).

### B. General model

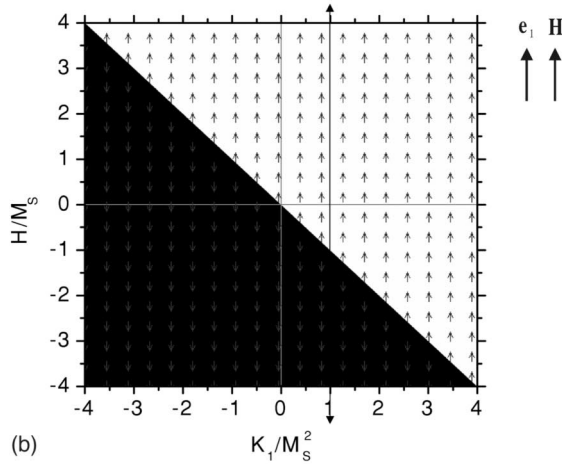
In the following we use a more general form of the free enthalpy, which includes unidirectional, uniaxial, and fourfold in-plane anisotropy contributions:

$$g = -K_1 \cos(\alpha_M) + K_2 \sin^2(\alpha_M - \alpha_2) + K_4 \sin^2(\alpha_M - \alpha_4) \cos^2(\alpha_M - \alpha_4) - HM_S \cos(\alpha_M - \alpha_H), \quad (1)$$

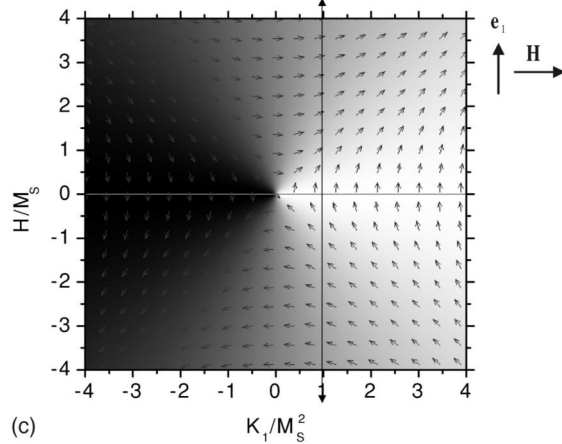
where  $K_1$ ,  $K_2$ , and  $K_4$  denote the unidirectional, uniaxial, and fourfold anisotropy constants, respectively. The easy direction of the unidirectional anisotropy for  $K_1 > 0$  is chosen as a reference for the definition of angles specifying the orientation of the applied field  $\alpha_H$ , the easy axis for the uniaxial anisotropy  $\alpha_2$ , and the fourfold anisotropy  $\alpha_4$ . These angles are defined by the geometry sketched in Fig. 2.



(a)



(b)



(c)

FIG. 1. (a) Magnetization reversal curves for unidirectional anisotropy with  $K_1/M_S^2=1$ . The external field is aligned parallel to the easy direction of the unidirectional anisotropy for the line and perpendicular for the symbols. The phase diagram of the system for parallel aligned field is given in (b) and for perpendicular aligned field in (c). White indicates parallel alignment of the magnetization direction with respect to the easy direction of the unidirectional anisotropy in (b) while black indicates antiparallel alignment. In the same manner the graylevel in (c) indicates the direction of the magnetization with respect to the easy direction of the unidirectional anisotropy.

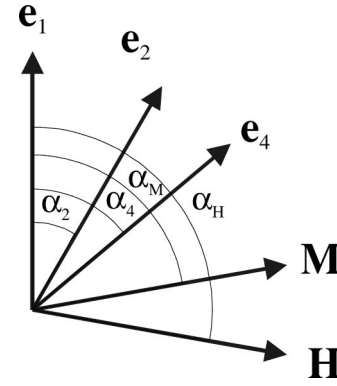


FIG. 2. Geometry of the system with unidirectional anisotropy including the direction of the magnetization, external field, uniaxial, and fourfold anisotropy with their corresponding in-plane angles  $\alpha_M$ ,  $\alpha_H$ ,  $\alpha_2$ , and  $\alpha_4$  with respect to the reference direction given by the unidirectional anisotropy.

$H$  is the strength of the external field and  $M_S$  is the saturation magnetization of the ferromagnetic layer.

Calculation of phase diagrams and magnetization reversal in the examples that follow is performed by minimizing the free enthalpy with respect to the angle of the magnetization  $\alpha_M$ . For the computation of magnetization reversal either the Maxwell convention or the perfect delay convention can be used.<sup>16</sup> By using the Maxwell convention it is assumed that the magnetization is always in the global minimum of the free enthalpy. On the other hand, the perfect delay convention assumes that the magnetization remains in the local minimum of the free enthalpy as long as this minimum exists. Therefore in the Maxwell convention there is no hysteretic behavior and the coercivity is always zero, whereas the perfect delay convention allows hysteresis and gives an upper limit for the coercivity.

### III. ANALYSIS OF BIASED SYSTEMS

In this section we first consider a system with a fixed unidirectional anisotropy  $K_1 > 0$  and a variable twofold anisotropy  $K_2$ . As a second case we analyze a system with a fixed unidirectional anisotropy  $K_1 > 0$  and a variable fourfold anisotropy  $K_4$ . For this case the influence of the direction of the applied magnetic field is discussed in detail. In the model we use, the role of the antiferromagnet is described implicitly through effective anisotropies, and no attempt is made to model effects of internal degrees of freedom of the antiferromagnet or interface spins. This means that the anisotropy “constants” are interpreted as measures of effective torques exerted by the antiferromagnet on the ferromagnet across the interface, and also include any anisotropies strongly modified, or due entirely, to the interface. By this we mean that on an atomic level the interface represents a chemical environment that is very different from other locations within the films. These differences generally reflect the lower atomic level symmetry of the interface region, a feature that by itself is in some cases sufficient to allow the formation of magnetic anisotropies that can differ significantly in type and magnitude from anisotropies far from interfaces. Related consider-

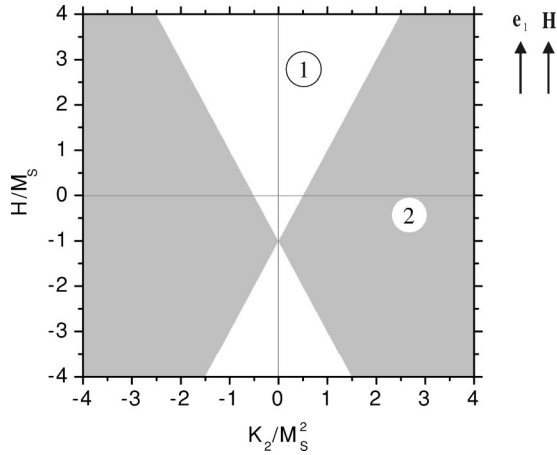


FIG. 3. Phase diagram of a system with fixed unidirectional anisotropy  $K_1/M_S^2=1$  and variable uniaxial anisotropy  $K_2$  with the field aligned along the easy direction of the unidirectional anisotropy. The phases with one and two minima in the free enthalpy are labeled 1 and 2 accordingly. For  $K_2>0$  the easy direction of the unidirectional anisotropy is parallel to the easy axis of the uniaxial anisotropy while for  $K_2<0$  the easy direction of the unidirectional anisotropy is parallel to the hard axis of the uniaxial anisotropy.

ations also explain modifications of anisotropies through strain induced directly by lattice mismatch at the interfaces. This also means that the constants may themselves be dependent upon either the ferromagnet or antiferromagnet thickness, and the magnetic history of the system.

For simplicity, we assume that the easy direction of the unidirectional anisotropy coincides with an easy direction of the higher-order anisotropy for  $K_i>0$   $i \in \{2,4\}$ . Notice that for  $K_i<0$  this geometry corresponds to a parallel alignment of a hard axis of the higher-order anisotropy and the easy direction of the unidirectional anisotropy.

**A. Influence of the magnitude of  $K_2$**

In a system with a unidirectional anisotropy  $K_1$  and a uniaxial anisotropy  $K_2$  the effects of applying the external magnetic field along the easy direction of the unidirectional anisotropy are shown in Fig. 3. The phase diagram is equivalent to the phase diagram of a system with a uniaxial anisotropy only but is shifted along the field axis by the amount of the exchange-bias field  $H_{eb} = -K_1/M_S$ . The details of these phase diagrams have been described already by Millev *et al.*<sup>14,15</sup> Their results can be directly adopted to the present case, but one should notice that we are considering in-plane anisotropies only. The effects of applying the external magnetic field perpendicular to the easy direction of the unidirectional anisotropy are shown in Fig. 4. In this case the phase diagram is strongly different compared to a uniaxial system without a unidirectional anisotropy. As the magnetic field is applied perpendicular to the easy direction  $e_1$  of the unidirectional anisotropy the phase diagram is not shifted on the field axis. Different magnitudes of the applied magnetic field not only change the magnitude but also the direction of the effective field  $H_{eff} = H + e_1 K_1/M_S$ , which acts on the magnetization and is composed of the applied magnetic field and the exchange-bias field.

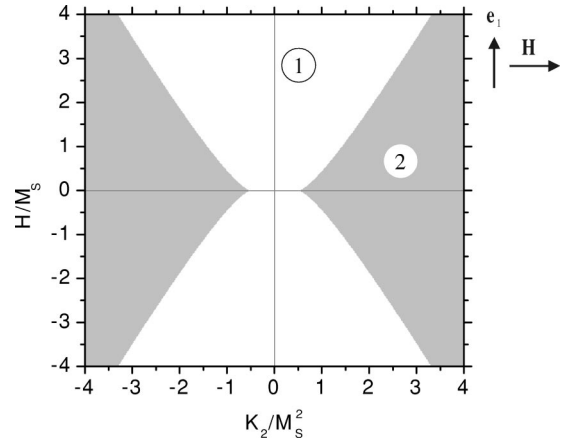


FIG. 4. Phase diagram of a system with fixed unidirectional anisotropy  $K_1/M_S^2=1$  and variable uniaxial anisotropy  $K_2$  with the field aligned perpendicular to the easy direction of the unidirectional anisotropy. The phases with one and two minima in the free enthalpy are labeled 1 and 2 accordingly.

**B. Influence of the magnitude of  $K_4$**

In the following we will further elaborate the concept of the phase diagrams by analyzing the case of a system with a unidirectional and a fourfold anisotropy in detail. Effects of applying the external magnetic field along the easy direction of the unidirectional anisotropy are shown in Fig. 5(a). The magnetization reversal exhibits a coercivity as expected for coherent rotation for a fourfold anisotropy of magnitude  $K_4$ . A discontinuous change of the magnetization direction accompanied by a discontinuous change of the free enthalpy of the system occurs as can be seen in Fig. 5(b). The reason for this can be understood by following the path of the magnetization reversal in the phase diagram shown in Fig. 6. This phase diagram has the same structure as a phase diagram for a system with a fourfold anisotropy only, but it is shifted

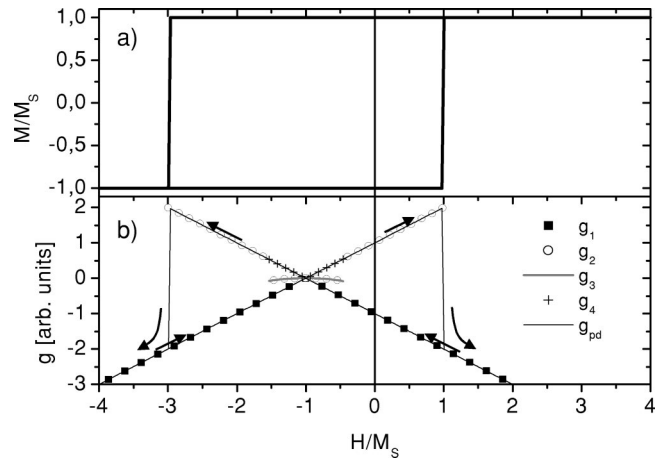


FIG. 5. (a) Magnetization reversal for a system with unidirectional and fourfold anisotropies with  $K_1/K_4=1$ , using the perfect delay convention. The field is applied along the easy direction of the unidirectional anisotropy. (b) Field dependence of the four different minima of the free enthalpy  $g_1, \dots, g_4$  and of the free enthalpy during reversal assuming perfect delay  $g_{pd}$ .

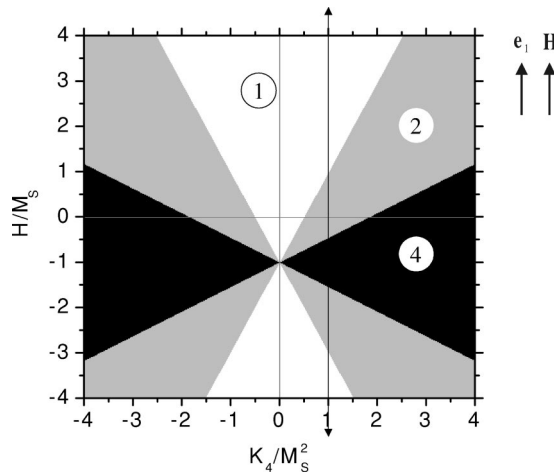


FIG. 6. Phase diagram of a system with fixed unidirectional anisotropy  $K_1/M_S^2=1$  and variable fourfold anisotropy  $K_4$  with the field aligned along the easy direction of the unidirectional anisotropy. The phases with one, two, and four minima in the free enthalpy are labeled 1, 2, and 4 accordingly. The position of the magnetization reversal given in Fig. 5 is indicated by a double arrow. Note that for  $K_4>0$  the easy direction of the unidirectional anisotropy is parallel to the easy axis of the fourfold anisotropy while for  $K_4<0$  the easy direction of the unidirectional anisotropy is parallel to the hard axis of the fourfold anisotropy.

along the field axis due to the presence of the unidirectional anisotropy. Three different phases can be seen in Fig. 6: phase 1 where only one minimum exists in the free enthalpy; and phases 2 and 4 where two and four minima of the free enthalpy exist.

The phase boundaries separating phase 1 and phase 2 are of special importance for the magnetization reversal shown in Fig. 5. In this case  $K_4>0$  and the transition from phase 2 to phase 1 with changing applied field occurs via an associated instability of the magnetic configuration. This is due to the discontinuous change of the free enthalpy which accompanies the discontinuous change of the magnetization direction. Note that there are possible states present in the phase diagram that may not be accessed during magnetization reversal. The reason is that the system remains in a local minimum until the configuration either becomes unstable, or thermal fluctuations are larger than the energy barrier stabilizing the state. A state such as that with enthalpy  $g_3$  in Fig. 5 can only be accessed by thermal excitation of the system over a relatively high-energy barrier.

No shift of the magnetization reversal along the field axis is observed if the magnetic field is applied perpendicular to the easy axis. Minor hysteresis loop features such as those shown in Fig. 7 appear depending on the ratio of the anisotropy constants ( $K_1/K_4=1$  in this figure). The reason for this complicated behavior is the different phases present in the system, where one, two, three, and four minima exist in the free enthalpy. The multiple minima for this choice of values are indicated in Fig. 8. The magnetization reversal process shown in Fig. 7 involves phases with one and two minima as follows. A new minimum appears in the region labeled “a” as the magnetic field is lowered after saturation in positive

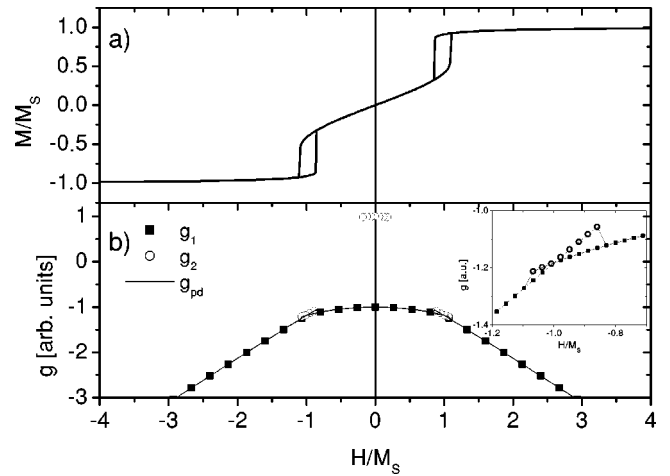


FIG. 7. (a) Magnetization reversal for a system with unidirectional and fourfold anisotropies with  $K_1/K_4=1$ . The field is applied perpendicular to the easy direction of the unidirectional anisotropy. (b) Field dependence of two different minima of the free enthalpy  $g_1$ ,  $g_2$  and of the free enthalpy during reversal assuming perfect delay  $g_{pd}$ , a magnified view for  $H=-1.2, \dots, -0.7$  is shown in the inset.

field. The enthalpy minimum  $g_2$ , in which the magnetization is in according to the perfect delay convention, becomes unstable when leaving region “a,” giving rise to the first discontinuous change in the magnetization shown in Fig. 7.

If the magnetic field is lowered further, the magnetization rotates and a new energy minimum appears in region “b.” This new minimum is at an energy higher than the state the magnetization is in and cannot therefore be accessed unless the energy of the magnetic system is increased. The configuration again becomes unstable as the field is changed and the system leaves region “c.” This appears as a second discon-

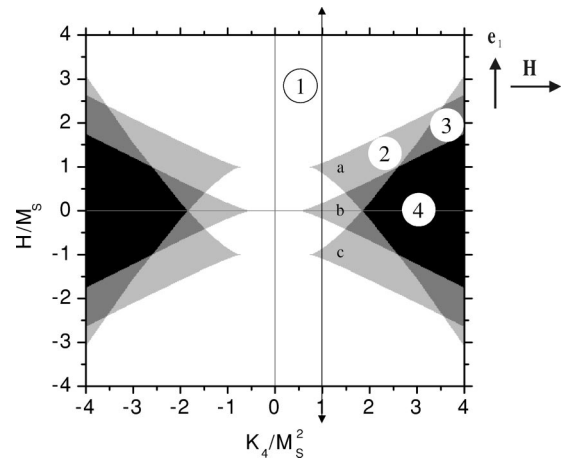


FIG. 8. Phase diagram of a system with fixed unidirectional anisotropy  $K_1/M_S^2=1$  and variable fourfold anisotropy  $K_4$  with the field aligned perpendicular to the easy direction of the unidirectional anisotropy. The phases with one, two, three, and four minima in the free enthalpy are labeled 1, 2, 3, and 4 accordingly. The position of the magnetization reversal given in Fig. 7 is indicated by a double arrow. The different parts of phase 2 crossed during this reversal are labeled a, b, and c.

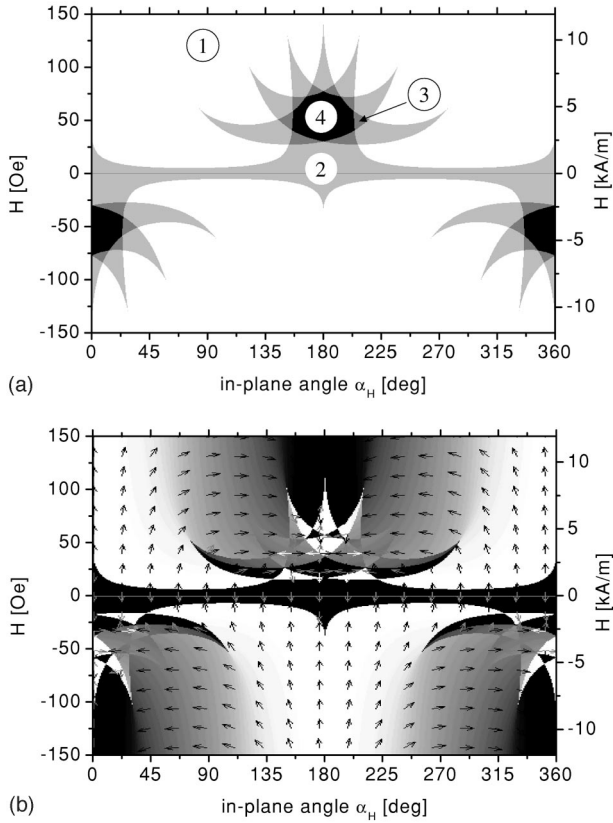


FIG. 9. Phase diagram for a system with unidirectional and four-fold anisotropy contributions ( $K_1=4.6 \times 10^4$  erg/cm<sup>3</sup> and  $K_4=3.8 \times 10^4$  erg/cm<sup>3</sup>) to the free enthalpy. In (a) the regions for which there exist one, two, three, or four minima are labeled 1, 2, 3, and 4, respectively. The arrows in (b) indicate the direction of the magnetization in the minima of the free enthalpy; a detailed description is given in the text.

tinuous change in Fig. 7. Because of symmetry, the system follows the same evolution in reverse as the field is increased from negative saturation.

**C. Influence of the direction of the applied field**

The phase diagram of the system can be calculated for different in-plane angles of the applied field  $\alpha_H$  and variable field strength  $H$  for a fixed set of anisotropy constants  $K_1$  and  $K_4$ . Examples are shown in Figs. 9(a) and 9(b). In these examples the anisotropy constants  $K_1=4.6 \times 10^4$  erg/cm<sup>3</sup> and  $K_4=3.8 \times 10^4$  erg/cm<sup>3</sup> are used to represent an epitaxial exchange coupled Ni<sub>81</sub>Fe<sub>19</sub>/Fe<sub>50</sub>Mn<sub>50</sub>(001) bilayer with values determined by fits to experimental data reported elsewhere.<sup>12</sup> Experimental results are shown in Fig. 10(a) for comparison.

The allowed magnetic phases are shown in Fig. 9(a). Different numbers of minima are present in the free enthalpy of the system and are indicated by graylevels. As discussed above, the phase boundaries are important for the magnetization reversal. The examination of how the system crosses these boundaries with changing the angle  $\alpha_H$  provides insight into the role of higher anisotropy contributions.

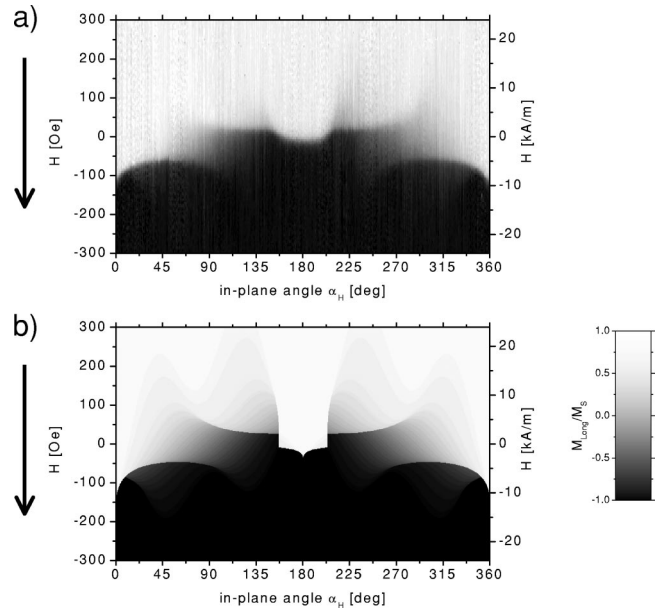


FIG. 10. Reversal diagram for the longitudinal component of the magnetization for the decreasing field branch (a) as measured for an epitaxial NiFe/FeMn bilayer system (Ref. 12) and (b) simulation for  $K_1=4.6 \times 10^4$  erg/cm<sup>3</sup> and  $K_4=3.8 \times 10^4$  erg/cm<sup>3</sup>. White corresponds to parallel alignment of the magnetization with respect to the positive field direction and black to antiparallel alignment. As indicated by the black arrow on the left, only the decreasing field branch is shown.

In Fig. 9(b) a detailed phase diagram is shown where the graylevel is proportional to the angle  $\alpha_{M,min}$  between the magnetization direction in the global minimum of the free enthalpy and the easy direction of the unidirectional anisotropy. Different regions of the phase diagram, where one, two, three, and four minima exist in the free enthalpy, are identified by the following graylevel convention. The number of minima in a given region is indicated by the numbers in Fig. 9(a). In Fig. 9(b) the level white in an odd number of minima region corresponds to  $\alpha_{M,min}=0^\circ$ , while black corresponds to  $\alpha_{M,min}=180^\circ$ . In a region with even number of minima white corresponds to  $\alpha_{M,min}=180^\circ$  while black corresponds to  $\alpha_{M,min}=0^\circ$ . The reason for this convention is to make contrast clear.

The magnetization directions in each minimum of the free enthalpy are indicated by small arrows. The graylevel of the arrows is chosen according to the free enthalpy of the corresponding minima. A black arrow indicates the magnetization direction with the lowest free enthalpy and a white arrow indicates the minimum with the highest free enthalpy.

In order to compare the simulations with the experimental data, the longitudinal component of the magnetization during magnetization reversal is indicated in the reversal diagram given in Fig. 10. White corresponds to parallel alignment of the magnetization with respect to the positive field direction, and black means that the magnetization is aligned antiparallel with the positive field direction. This convention is used for both the experimental data shown in Fig. 10(a) and the calculation results shown in Fig. 10(b).

Comparison of Figs. 10(a) and 10(b) shows very good agreement between experiment and the effective anisotropy model discussed here. Note that discontinuous changes of the magnetization occur only at phase boundaries and that the sharp edges in the simulation appear to be somewhat blurred in the experiment. In particular, note that the peak at  $0^\circ$  is present in both calculation and experiment whereas the peak at  $180^\circ$  of the calculation is not present in the experimental data in Fig. 10(a). Reasons for the blurring of edges and other differences in the fine structure of the reversal diagrams may be related to thermal effects. These are discussed in the following section.

#### IV. STABILITY AND ENERGY BARRIERS

##### A. The role of barriers for metastable states

In this section we consider the role of the energy barriers for a metastable state. As discussed above, evolution of the magnetization under the so-called perfect delay convention assumes that the magnetization remains in a metastable state as long as there is an energy barrier present separating the local enthalpy minimum from other enthalpy minima corresponding to other, possibly lower, enthalpy configurations. Thermal fluctuations are one way in which the magnetic system can change from one such minimum to another.<sup>17</sup> Following Néel, one can think of thermal fluctuations affecting the magnetic system as effective magnetic fields that appear randomly throughout the sample at random times, with random orientation.<sup>18,19</sup> The magnetization will react to the torque produced by the transient field, and may reorient if the field is large enough. In this way a Langevin type torque equation can be constructed and used to represent the thermal “buffeting” of local magnetization one expects for a magnetic system at equilibrium at finite temperature. Note also that thermal processes may be associated primarily with the antiferromagnet and modify locally the anisotropy fields and constants acting on the ferromagnet. The exact manner in which this can occur is dependent on the microscopic mechanisms governing the formation of the effective anisotropies acting on the ferromagnet.

The stability of the system in the local minimum of the free enthalpy  $g_{local,min}$  was examined by calculating the barrier height  $e_{1,2}(H) = g_{max\ 1,2} - g_{local,min}$ , where  $g_{max\ 1,2}$  are the adjacent maxima in the free enthalpy relative to the local enthalpy minimum. The distribution of thermal fluctuations below the ordering temperature is assumed to obey Boltzmann statistics, so that it is more likely within a given time interval for the system to hop over a barrier from a high enthalpy state to a low enthalpy state than it is for the reverse process to occur and the system enthalpy to increase. As such, we focus our discussion on thermal processes that lower the system enthalpy and define the energy barrier as the minimum barrier taking the system from one configuration to another:  $e(H) = \min[e_1(H), e_2(H)]$ .

In Fig. 11(a) the dependence of this barrier height on the field strength is shown for the system investigated in the preceding section. The field is applied antiparallel to the easy direction of the unidirectional anisotropy at  $\alpha_H = 180^\circ$ . The barrier height covers a wide range of energy densities and is

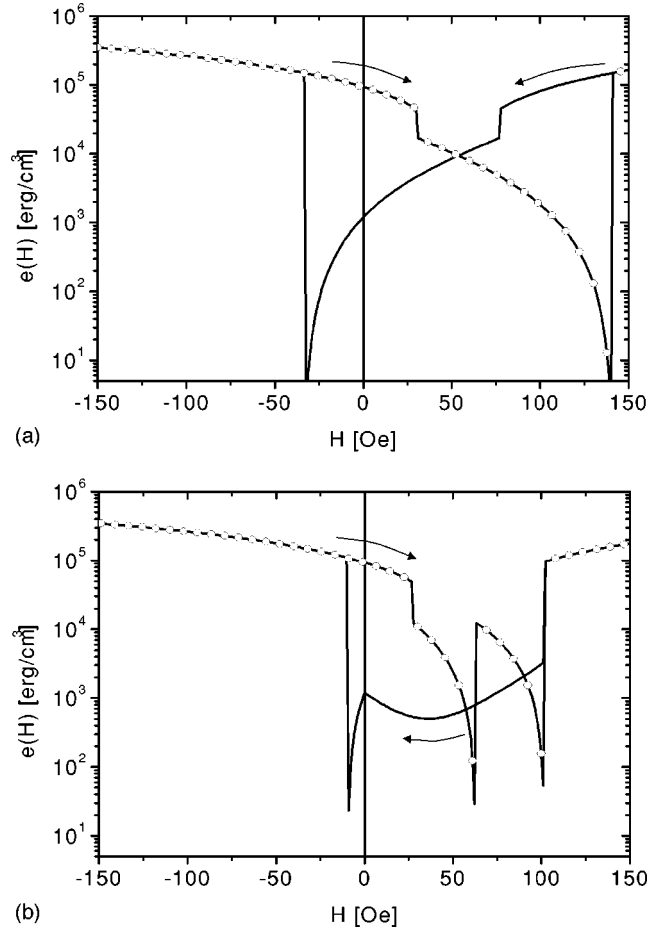


FIG. 11. Barrier height  $e(H)$  for (a) an angle of the applied field of  $\alpha_H = 180^\circ$  (i.e., along the unidirectional easy axis) and (b) for  $\alpha_H = 160^\circ$ . Open symbols correspond to increasing field and the line corresponds to decreasing field as also indicated by the arrows.

therefore shown on a logarithmic scale. Due to the symmetry of the problem the barrier height is the same for the increasing and decreasing field branch of the magnetization reversal with respect to the exchange-bias field. This is no longer true if the field is applied in a direction that is not collinear with respect to the easy direction of the unidirectional anisotropy.

The field dependence of the barrier height is shown in Fig. 11(b) for  $\alpha_H = 160^\circ$ . In this case the barrier height becomes asymmetric for both branches of the magnetization reversal in that the barrier height is different when the field is increased from negative saturation compared to the situation when the field is decreased from positive saturation. Therefore any process that is sensitive to the barrier height will become asymmetric in this sense. This has been discussed in the context of time- and temperature-dependent processes by several authors,<sup>20–22</sup> and may be related to domain orientation asymmetry observed during the magnetization reversal.<sup>23–25</sup>

##### B. Thermal activation

Following Street and Woolley,<sup>17</sup> the probability for a thermally activated lowering of the system enthalpy depends on

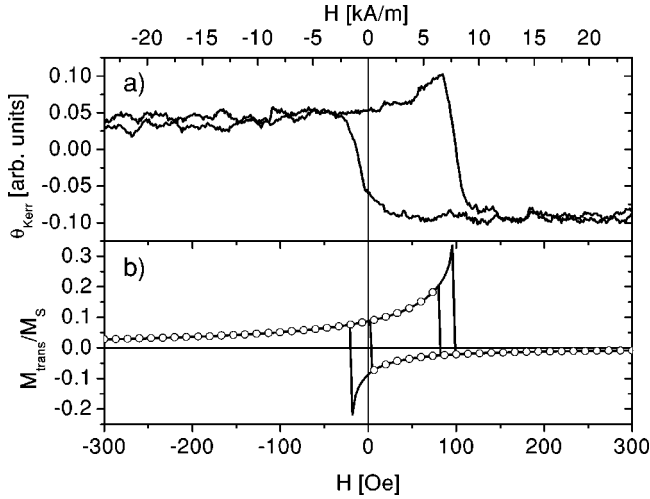


FIG. 12. Transversal component of the magnetization for  $\alpha_H = 175^\circ$  (a) as measured for an epitaxial NiFe/FeMn bilayer (Ref. 12) and (b) as predicted by the Stoner-Wohlfarth model for  $K_1 = 4.6 \times 10^4$  erg/cm<sup>3</sup> and  $K_4 = 3.8 \times 10^4$  erg/cm<sup>3</sup> without thermal activation (line) and with thermal activation for  $e_{therm} = 1300$  erg/cm<sup>3</sup> (open symbols).

time interval  $\Delta t$  and barrier energy  $E_B$  according to  $P(\Delta t) \sim 1 - \exp[-(\Delta t/\tau)\exp(-E_B/k_B T)]$ , where  $1/\tau$  denotes the attempt frequency. We approximate this with a Heaviside step function by  $P(\Delta t) = \Theta(k_B T - E_B)$  under the assumption that  $\Delta t/\tau$  is not too large, with  $k_B T$  not too large compared with  $E_B$ . This means that all processes associated with energy barriers below a certain cutoff defined by  $k_B T$  occur. Such an approximation provides a crude picture of what one might expect for very narrow energy barrier distributions and quasistatic hysteresis loop measurements.

The idea is that if the temperature is low, there are only a few possibilities for the system to spontaneously switch from one configuration to a lower enthalpy configuration. This will occur whenever one of the barrier heights  $e_1(H)$  or  $e_2(H)$  separating the local minimum from the adjacent ones is less than a given thermal energy density  $e_{therm}$ . The influence of thermal activation on the transversal component of the magnetization during reversal in this picture is shown in Fig. 12(b) for an in-plane angle of the applied field  $\alpha_H = 175^\circ$ . Magnetization reversal without the possibility of thermal activation is shown as a reference. In Fig. 12(a) the corresponding experimental data are shown. The cutoff for this case is set such that energy barriers less than 1300 erg/cm<sup>3</sup> are allowed to be overcome.

Notice that the transversal component of the magnetization has been chosen because the Stoner-Wohlfarth model predicts an ongoing rotation of the magnetization for this angle. This has a very clear signature in the transversal component of the magnetization and can be seen in Fig. 12(b). However, experimentally<sup>12</sup> we did only observe one of the two characteristic peaklike structures in the transversal component of the magnetization, compare Fig. 12(a). In Figs. 13(a)–13(c) the angular dependences of the magnetization reversal for temperatures corresponding to  $e_{therm} = 1000$ , 1300, and 1700 erg/cm<sup>3</sup> are shown. In comparison with the

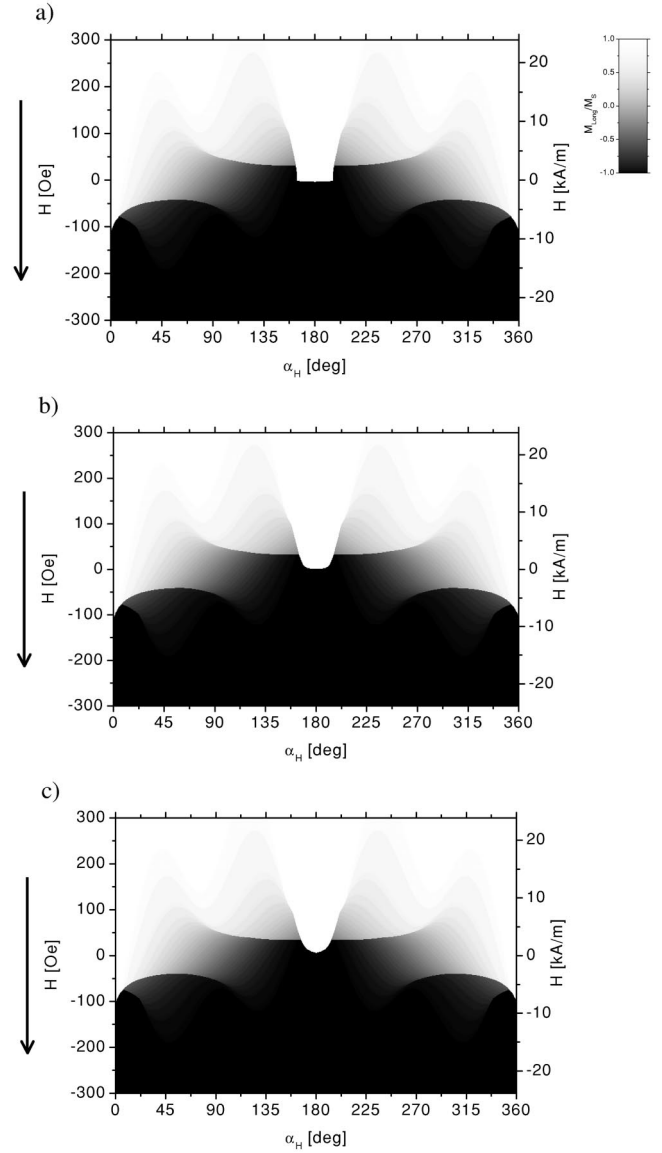


FIG. 13. Simulation of the longitudinal component of the magnetization for the decreasing field branch (indicated by the black arrow on the left) of the magnetization reversal for a system with  $K_1 = 4.6 \times 10^4$  erg/cm<sup>3</sup> and  $K_4 = 3.8 \times 10^4$  erg/cm<sup>3</sup> including thermal activation and (a)  $e_{therm} = 1000$  erg/cm<sup>3</sup>, (b)  $e_{therm} = 1300$  erg/cm<sup>3</sup>, and (c)  $e_{therm} = 1700$  erg/cm<sup>3</sup>.

case without thermal activation the sharp edges are rounded out with increasing temperature resulting in a better agreement between simulation and experiment. Especially, the structure at  $\alpha_H = 180^\circ$  that is present in the calculation without thermal activation shown in Fig. 10 (lower panel) but not in the experiment of Fig. 10 (upper panel) vanishes when thermal activation is included, as can be seen in Fig. 13. The peak at  $\alpha_H = 0^\circ$  is still present and is only reduced in size—as observed in the experiment. As all experiments were done at 293 K from the measurements a rough estimation of the activation volume involved,  $V$ , can be made for  $e_{therm} = kT/V \approx 1300$  erg/cm<sup>3</sup>. This results in an activation volume of  $2.3 \times 10^{-23}$  m<sup>3</sup>, which corresponds to a cylinder with a radius  $r \approx 40$  nm. This is of the same order as the

exchange length ( $l_{ex} \approx \sqrt{A/K}$ , with  $A$  the exchange stiffness and  $K$  the anisotropy constant) and is therefore consistent with the Stoner-like thermal switching assumed for these estimates of thermal activation.

## V. SUMMARY

We have presented a detailed discussion of the influence of the magnitude of higher-order anisotropy contributions in exchange-biased systems. We have introduced the use of phase diagrams for exchange-biased systems and shown how these allow one to trace the magnetization reversal for a variety of anisotropy strengths and applied field orientations. The boundaries separating different phases are critical as the local minimum in which the system is in can become unstable, giving rise to a discontinuous change of the magnetization.

The analysis of the energy barriers separating a local minimum from neighboring minima shows that higher-order anisotropy contributions to these barriers become strongly asymmetric if the field is not applied along a high symmetry direction. Therefore including thermal activation in the simu-

lation for magnetization reversal has a different influence on the forward and reverse branches of a magnetization loop measurement, and may therefore account for the observed systematic deviations between experiment and calculations without thermal activation.

Further experimental work is clearly needed in order to demonstrate the exact dependence on temperature of the forward and reverse field asymmetry. The measurements are extremely time consuming and interpretation of the data is further complicated by temperature dependences of the magnetic anisotropy energies themselves. In particular, the ratio of  $K_4$  to  $K_1$  is temperature dependent, thereby making the energy barriers themselves dependent on temperature. Work along these lines is in progress.

## ACKNOWLEDGMENTS

The authors would like to thank R. Street for stimulating and fruitful discussions. J.V.K. and R.L.S. were supported by the Australian Research Council. T.M. acknowledges support by the Studienstiftung des Deutschen Volkes.

- 
- <sup>1</sup>W.H. Meiklejohn and C.P. Bean, Phys. Rev. **102**, 1413 (1956).  
<sup>2</sup>W.H. Meiklejohn and C.P. Bean, Phys. Rev. **105**, 904 (1957).  
<sup>3</sup>J. Nogués and I.K. Schuller, J. Magn. Magn. Mater. **192**, 203 (1999).  
<sup>4</sup>A.E. Berkowitz and K. Takano, J. Magn. Magn. Mater. **200**, 552 (1999).  
<sup>5</sup>R.L. Stamps, J. Phys. D **33**, R247 (2000).  
<sup>6</sup>E.C. Stoner and E.P. Wohlfarth, Philos. Trans. R. Soc. London, Ser. A **240**, 599 (1948).  
<sup>7</sup>H. Xi, M.H. Kryder, and R.M. White, Appl. Phys. Lett. **74**, 2687 (1999).  
<sup>8</sup>H.J. Santos, F.A. Pinheiro, A.Y. Takeuchi, L.C. Sampaio, R.A. Simao, C.A. Achete, and M. Cremona, Phys. Rev. B **60**, 68 (1999).  
<sup>9</sup>T. Pokhil, E. Linville, and S. Mao, J. Appl. Phys. **89**, 6588 (2001).  
<sup>10</sup>C.-H. Lai, Y.-H. Wang, C.-R. Chang, J.-S. Yang, and Y.D. Yao, Phys. Rev. B **64**, 094420 (2001).  
<sup>11</sup>Y.J. Tang, B.F.P. Roos, T. Mewes, M. Bauer, S.O. Demokritov, B. Hillebrands, and W.S. Zhan, Mater. Sci. Eng., B **76**, 59 (2000).  
<sup>12</sup>T. Mewes, H. Nembach, M. Rickart, S.O. Demokritov, J. Fassbender, and B. Hillebrands, Phys. Rev. B **65**, 224423 (2002).  
<sup>13</sup>M.J. Pechan, D. Bennett, N. Teng, C. Leighton, J. Nogués, and I.K. Schuller, Phys. Rev. B **65**, 064410 (2002).  
<sup>14</sup>Y.T. Millev, H.P. Oepen, and J. Kirschner, Phys. Rev. B **57**, 5837 (1998).  
<sup>15</sup>Y.T. Millev, H.P. Oepen, and J. Kirschner, Phys. Rev. B **57**, 5848 (1998).  
<sup>16</sup>S. Nieber and H. Kronmueller, Phys. Status Solidi B **165**, 503 (1991).  
<sup>17</sup>R. Street and J.C. Woolley, Proc. Phys. Soc. London **62**, 562 (1949).  
<sup>18</sup>L. Néel, J. Phys. Radiat. **11**, 49 (1950).  
<sup>19</sup>L. Néel, J. Phys. Radiat. **12**, 339 (1951).  
<sup>20</sup>E. Fulcomer and S.H. Charap, J. Appl. Phys. **43**, 4190 (1972).  
<sup>21</sup>R.L. Stamps, Phys. Rev. B **61**, 12 174 (2000).  
<sup>22</sup>A.M. Goodman, K. O'Grady, M.R. Parker, and S. Burkett, J. Magn. Magn. Mater. **193**, 504 (1999).  
<sup>23</sup>M.R. Fitzsimmons, P. Yashar, C. Leighton, I.K. Schuller, J. Nogués, C.F. Majkrzak, and J.A. Dura, Phys. Rev. Lett. **84**, 3986 (2000).  
<sup>24</sup>C. Leighton, M. Song, J. Nogués, M.C. Cyrille, and I.K. Schuller, J. Appl. Phys. **88**, 344 (2000).  
<sup>25</sup>I.N. Krivorotov, C. Leighton, J. Nogués, I.K. Schuller, and E. Dan Dahlberg, Phys. Rev. B **65**, 100402(R) (2002).